JACS Au
AN OPEN ACCESS JOURNAL OF THE AMERICAN CHEMICAL SOCIETY

pubs.acs.org/jacsau

Article

Photoactive Fe Catalyst for Light-Triggered Alkyd Paint Curing

Johan Bootsma, Wesley R. Browne, Jitte Flapper, and Bas de Bruin*

Cite This: *JACS Au* 2022, 2, 531–540

Read Online

ACCESS | Metrics & More | Article Recommendations | Supporting Information

ABSTRACT: Herein, we show that the photoactive complexes $[(Cp)Fe(arene)]^+$ (Cp = cyclopentadienyl; arene = C_6H_6, C_6H_5Me) act as latent catalysts that allow for photochemical control over the onset of alkyd paint curing, without the need for antiskinning agents such as the volatile 2-butanone oxime normally used to prevent curing during paint storage. The highly soluble neutral complexes [(Cp)Fe(Ch)] and [(Cp)Fe(Ch′)] (Ch = cyclohexadienyl, Ch′ = methylcyclohexadienyl) readily convert to the photoactive complexes $[(Cp)Fe(arene)]^+$ upon oxidation in alkyd, allowing the latter to be dosed in a wide range of concentrations. Infrared and Raman studies show similar spectral changes of the alkyd paint matrix as have been observed in alkyd curing mediated by well-known, industrially applied cobalt- and manganese-based catalyst $Co(neodecanoate)_2$ and $[(Me_3TACN)_2Mn_2(\mu\text{-}OOCR)_3](OOCR)$. The $[(Cp)Fe(Ch)]/[(Cp)Fe(arene)]^+$ system performs equally well as these cobalt- and manganese-based catalysts in terms of drying time and outperform the manganese catalyst by showing a hardness development (increase) similar to that of the cobalt-based catalyst. Based on electron paramagnetic resonance and light−activity studies, we propose that photolysis of $[(Cp)Fe(arene)]^+$ generates short-lived active Fe^{II} species, explaining the desired latency. The $[(Cp)Fe(Ch)]/[(Cp)Fe(arene)]^+$ alkyd curing systems presented herein are unique examples of intrinsically latent paint curing catalysts that (1) are based on an abundant and harmless transition metal (Fe), (2) do not require any antiskinning agents, and (3) show favorable performance in terms of drying times and hardness development.

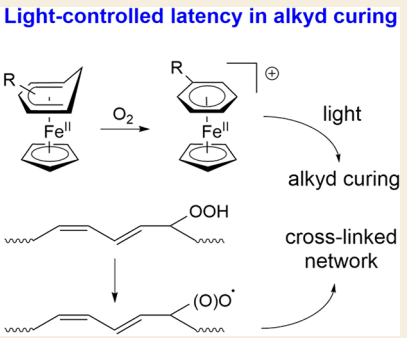

KEYWORDS: *(photo)latency, alkyd curing, radical cross-linking, high-spin $(Cp)Fe^{II}$, cobalt replacement, antiskinning agent-free, hard coatings*

INTRODUCTION

Stimuli-responsive catalysts are attracting increasing attention to achieve spatial and temporal control of chemical transformations,[1] mimicking metabolic processes in living cells.[2] Stimuli-responsive catalysts also provide ample opportunities in external control of properties in material science, with photoswitching being an especially attractive functionality for future applications.[3] Indeed, light-sensitive compounds and photocatalysts are used widely to initiate polymerization reactions.[4−6] Light-triggered activation of latent catalysts holds tremendous potential in the amplification of external triggers but has received limited attention in achieving latency in polymer cross-linking processes,[7] which is of particular importance to cure paint.

Alkyd resins are polyesters containing (unsaturated) fatty acids[8] that are produced predominantly from biorenewable resources on a multiton scale annually for use as the binder in industrial, domestic, and artist paints. Curing of alkyd paints involves a radical-based cross-linking process, based on the in situ formation and activation of (hydro)peroxides formed from (poly)unsaturated fatty acids and air oxygen (Scheme 1).[9−11] The noncatalyzed process is slow and can take days or even weeks to complete. Hence, catalysts are added based primarily on cobalt, vanadium, iron, and manganese.[12]

Currently, the main drier combination used for alkyd curing is based on cobalt carboxylates to increase the drying speed, with calcium and zirconium carboxylates added to increase stability and cross-link density, respectively.[13] Premature curing during storage, which leads to the formation of a thick polymeric layer known as a "skin" on the surface of the coating (often observed in old paint cans), is inhibited by adding antiskinning/blocking agents such as the volatile 2-butanone oxime, which inactivates the catalyst during storage.

However, while effective, the use of both cobalt and 2-butanone oxime in paints and coatings is under legislative pressure by programs such as the European REACH Regulation,[14] driving the replacement of cobalt and 2-butanone oxime by other (existing) catalysts and antiskinning methods. Other challenges, including yellowing of the cured films over time, the desire to move away from volatile organic compounds used as diluents, and the ambition to increase material properties by the hybridization of alkyds with other functionalized

Received: December 23, 2021
Published: January 27, 2022

https://doi.org/10.1021/jacsau.1c00579
JACS Au 2022, 2, 531−540

Scheme 1. Generally Accepted Mechanism of Alkyd Curing (Cross-Linking) Using Cobalt-Based Catalysts[9−11]

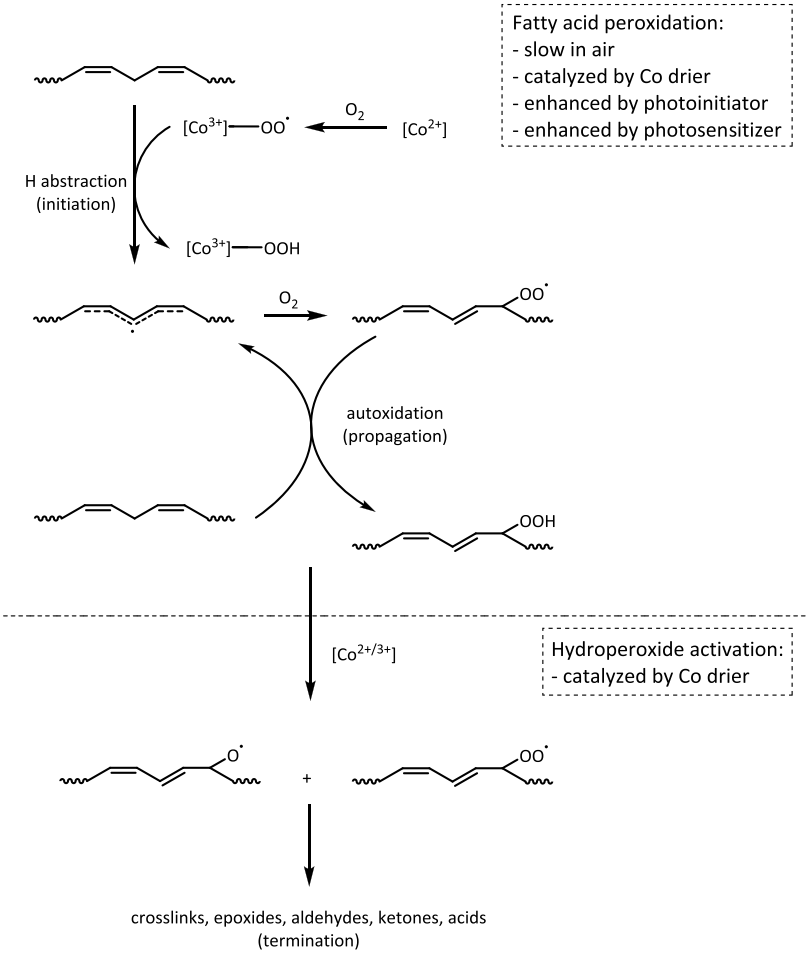

polymers (epoxy, acrylate, silicone, urethane, amide) further make alkyd coatings an interesting field of study.[15]

Alternative catalysts developed during the past 10 years, such as manganese complexes based on the Me_3TACN (*N*,*N*′,*N*″-trimethyl-1,4,7-triazacyclononane) ligand and iron complexes based on the bispidon ligand[16,17] emerged from their application in oxidative bleaching and stain removal catalysis.[18] Although these catalysts are effective in reducing the curing time, the cured films have a (final) hardness much lower than that in films cured with Co-based driers.[16] More recently, ferrocene and its substituted analogues,[19] in particular, acyl-substituted ferrocenes such as benzoyl ferrocene,[20] have also shown good performance. Their reactivity in alkyd curing is ascribed to the ferrocene/ferrocenium redox couple by analogy to the Co^{2+}/Co^{3+} cycle proposed for cobalt-based catalysts (Scheme 1).[11] However, their strong color makes their use in light-colored coatings less attractive.

Because paint is stored in closed cans, this provides a dark environment during storage, and we, therefore, considered light activation an interesting latency strategy to investigate. Previous work had already shown that the addition of photoinitiators[21−23] and/or photosensitizers[23,24] such as bis(2,6-difluoro-3-(1-hydropyrrol-1-yl)phenyl)titanocene ($[(Cp)_2Ti(Ar_F)_2]$), phenylbis(2,4,6-trimethylbenzoyl)phosphine oxide (BAPO), 1,2-diphenylethane-1,2-dione (benzil), 2-isopropylthioxanthone (ITX), rose bengal, and methylene blue (see Scheme 2 for structures) can fasten the curing, but these approaches still required the use of either cobalt-based driers[22−24] or the iron/bispidon complex,[21] for which no suitable antiskinning method has been developed (addition of 2-butanone oxime does not work well[16]). To the best of our knowledge, no systems have been reported that use light activation of the catalyst as a source of latency.

Herein, we report that the complex [(η^5-cyclopentadienyl)(η^5-cyclohexadienyl)iron] ([(Cp)Fe(Ch)]) and its methylated derivative [(η^5-cyclopentadienyl)(η^5-methylcyclohexadienyl)-iron] ([(Cp)Fe(Ch′)]) act as efficient visible-light-dependent catalysts for alkyd paint curing when mixed with alkyd paints under aerobic conditions (Scheme 3). This approach introduces latency through light activation, thus eliminating the need for antiskinning agents such as 2-butanone oxime. The new catalysts show excellent performance in terms of drying times and hardness development.

RESULTS AND DISCUSSION

Application of [(Cp)Fe(C_6H_6)](PF_6) (1) and [(Cp)Fe(C_6H_5Me)](PF_6) (1′) as Catalysts for the Curing of Setal-270

The class of $[(Cp)Fe(arene)]^+$ complexes, which can be prepared from ferrocene and $AlCl_3$ with the arene present in excess,[25] has been used previously for photo-cross-linking of epoxy resins.[26] The thermal and oxidative stability of these compounds,[25] as well as the absence of strong coloring (which is important for application in paint), prompted us to evaluate their potency in alkyd paint curing.

https://doi.org/10.1021/jacsau.1c00579
JACS Au 2022, 2, 531−540

Scheme 2. Examples of Photoinitiators and Photosensitizers Used Previously to Speed-up Alkyd Curing When Combined with Traditional Driers[21−24]

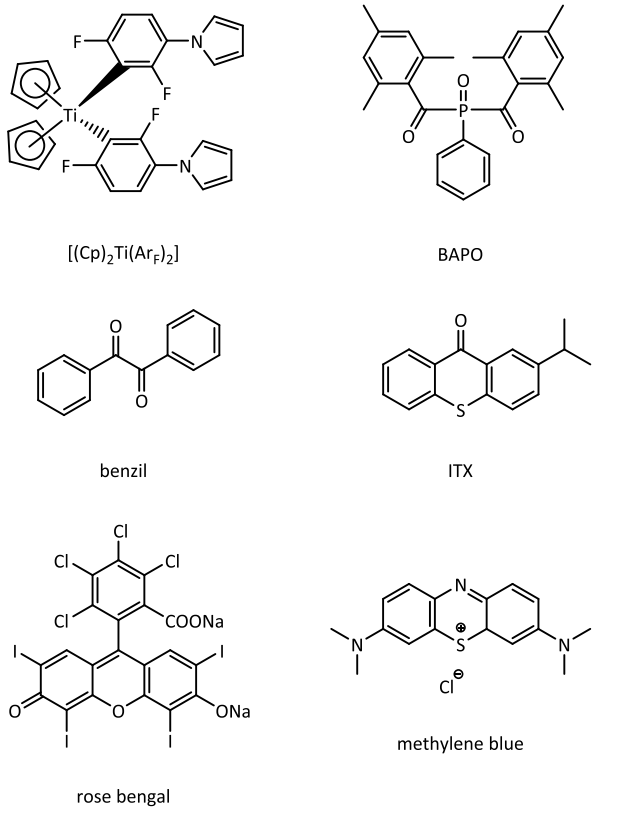

Scheme 3. Aerobic Oxidation of [(Cp)Fe(Ch)] (R = H) or [(Cp)Fe(Ch′)] (R = CH_3) Leads to in Situ Formation of the Corresponding $[(Cp)Fe(arene)]^+$ Complexes, Which Generate Active Fe^{II} Catalysts for Alkyd Paint Curing upon Photoactivation (L = alkyd donor/substrate)

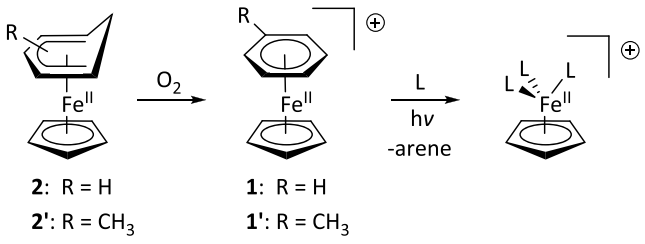

Initial studies examined the potency of the ionic compounds $[(Cp)Fe(C_6H_6)](PF_6)$ (**1**) and $[(Cp)Fe(C_6H_5Me)](PF_6)$ (**1′**) in the soybean-based alkyd Setal-270. Complex **1**, predissolved in acetone (see the Supporting Information), is soluble in alkyd mixtures in concentrations up to 0.05 wt % Fe with regard to solid binder content, above which precipitation takes place. (From here on, all concentrations will be given as wt % metal with regard to solid binder content; also see the Supporting Information.) Complex **1′**, also predissolved in acetone, was more soluble, and the dosage of this compound could be easily doubled to 0.10 wt % Fe. Notably, addition of **1** or **1′** leads to much less coloration than in the case of benzoylferrocene[19c,20a] (Figure 1).

The drying time for 90 μm thick films of alkyd mixtures containing **1** or **1′** under ambient lighting (fluorescent beam lighting + outdoor sunlight through the lab window)[27] becomes

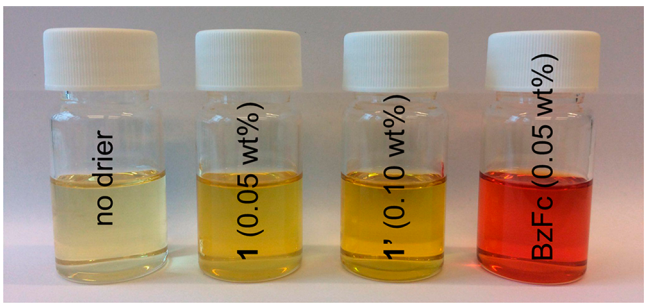

Figure 1. Addition of the complex $[(Cp)Fe(C_6H_6)](PF_6)$ (**1**) at 0.05 wt % (wt % metal with regard to solid binder content; see main text) or $[(Cp)Fe(C_6H_5Me)](PF_6)$ (**1′**) at 0.10 wt % leads to a slightly more yellow color with regard to the pure alkyd. Notably, addition of benzoylferrocene (BzFc) at 0.05 wt % leads to much stronger coloration. The complexes were dosed as solution in acetone.

shorter with increasing (pre)catalyst concentrations (6−7 h at 0.05 wt % **1**, 5 h at 0.10 wt % **1′**). Importantly, drying of 90 μm thick films dosed with **1** or **1′** did not take place in the dark (>24 h), and mixtures of $[(Cp)Fe(arene)](PF_6)$ in Setal-270 stored in the dark (in absence of 2-butanone oxime) did not develop a skin. These data demonstrate that **1** and **1′** act as a latent, photoactivated catalyst in alkyd paint curing. On the contrary, 90 μm thick films of alkyd mixtures dosed with benzoylferrocene cured in the dark just as fast as in the light, showing that, although effective, benzoylferrocene is not a photolatent alkyd drier. The light-triggered $[(Cp)Fe(arene)]^+$ catalysts are thus clearly distinct from all other reported paint driers.

In search for the possibility to dose the drier without the need of polar solvents to predissolve the charged complexes, we also investigated the possibility of in situ formation of $[(Cp)Fe(arene)]^+$ in a soluble form in the resin from a much more soluble (neutral) precursor.

In Situ Formation of $[(Cp)Fe(arene)]^+$ from [(Cp)Fe(Ch)] (2) and [(Cp)Fe(Ch′)] (2′)

Reduction of **1** with $LiAlH_4$[28] or $NaBH_4$[29] provides the neutral compound $[(\eta^5\text{-cyclopentadienyl})Fe(\eta^5\text{-cyclohexadienyl})]$ (**2**). Similarly, reduction of **1′** provides the neutral compound $[(\eta^5\text{-cyclopentadienyl})Fe(\eta^5\text{-methylcyclohexadienyl})]$ (**2′**).[30] In contrast to **1** and **1′**, complexes **2** and **2′** are highly soluble in aliphatic media and can even be dissolved in alkyd resin without additional solvent. Upon mixing a heptane solution of **2** or **2′** with Setal-270, a fast color change from red to yellow takes place, suggesting aerobic oxidation of the neutral complex to the cationic complex at room temperature.[31]

The solubility and in situ oxidation of **2** in Setal-270 in the concentration range of 0.02−0.14 wt % of Fe was determined by UV/vis absorption spectroscopy. Precipitation was not observed, and the absorption spectra show the conversion of the neutral complex [(Cp)Fe(Ch)] (λ_{max} = 414 nm) to the cationic complex $[(Cp)Fe(C_6H_6)]^+$ (λ_{max} = 452 nm) (Figure 2). Both the spectra and linear fits of the Lambert−Beer law plots (slope: 6.0 vs 6.1 for Setal-270 dosed with **2** and **1**, respectively) unambiguously support the in situ transformation of **2** to $[(Cp)Fe(C_6H_6)]^+$ (see Scheme 3).

When **2** (η^5-C_5H_5: 4.27 ppm) was mixed with a degassed solution of Setal-270 in heptane in a N_2-filled glovebox, only minor oxidation to the cationic complex (η^5-C_5H_5: 4.93 ppm) was observed (presumably due to oxidation by fatty acid peroxides slowly formed during storage of the alkyd). ^{1}H NMR analysis in $CDCl_3$ of a sample exposed to air overnight, on the

https://doi.org/10.1021/jacsau.1c00579
JACS Au 2022, 2, 531−540

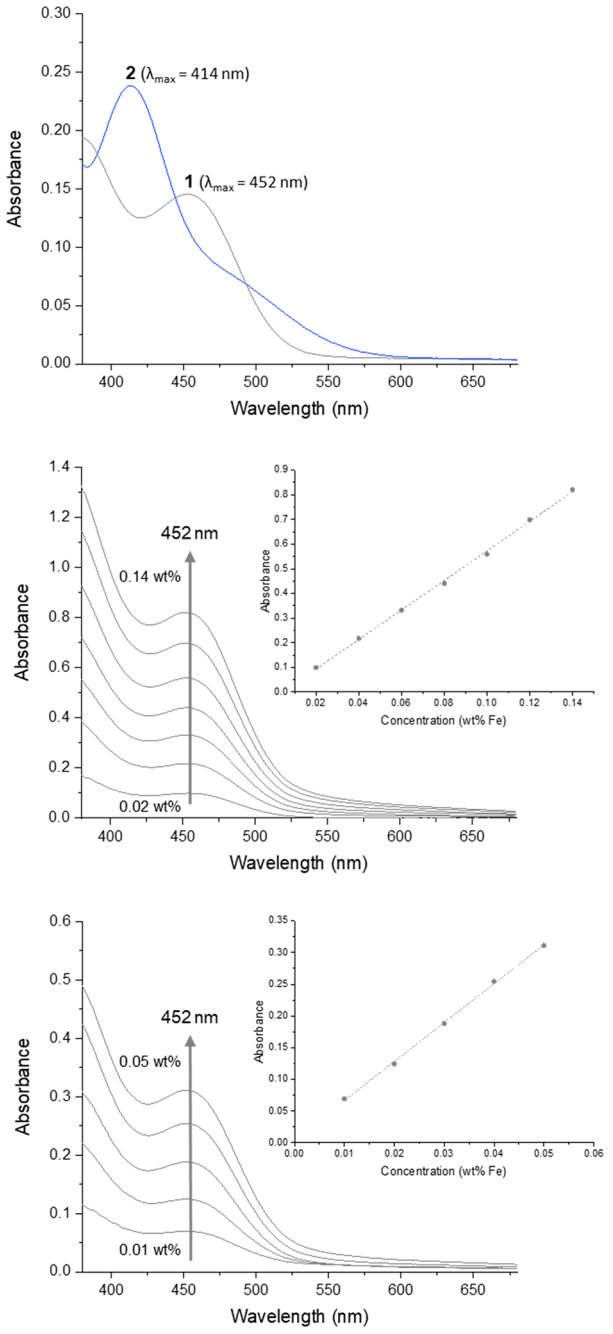

Figure 2. UV/vis absorption spectra of (top) **1** and **2** in CH_3CN and hexane, respectively, (middle) Setal-270 dosed with **2** (0.02−0.14 wt % Fe) and (bottom) Setal-270 dosed with **1** (0.01−0.05 wt % Fe). Measurements were performed under aerobic conditions.

other hand, showed broadened signals around 6.30 ppm (η^6-C_6H_6) and 5.08 ppm (η^5-C_5H_5) and disappearance of the signals belonging to **2**, indicating complete transformation of [(Cp)Fe(Ch)] to $[(Cp)Fe(C_6H_6)]^+$ (Figure S5).

Drying Time Performance and Time-Resolved Fourier Transform Infrared (FTIR) Spectroscopy and Raman Spectroscopy

Using the neutral precursors, drying times of 4 h were attainable for alkyd mixtures dosed with 0.10 wt % **2** or 0.12 wt % **2′**; the need for a slightly higher dosage of **2′** can be explained by the slightly lower quantum yield of photolysis of $[(Cp)Fe(C_6H_5Me)]^+$ compared to that of $[(Cp)Fe(C_6H_6)]^+$.[32]

Drying times for full formulations (including zirconium and calcium carboxylates; see the Supporting Information for full details) also showed that the rate of curing increases upon increasing the concentration of **2**, with drying times of ∼3 h for concentrations ≥0.10 wt % (Figure S3). These drying times are comparable to those for the well-known catalysts Co(neodecanote)$_2$ (CoNeo, **3**) and $[(Me_3TACN)_2Mn_2(\mu\text{-}OOCR)_3](OOCR)$ (Mn/MeTACN, **4**) (OOCR = acetate or 2-ethylhexanoate; see Supporting Information for full details), which are typically dosed at 0.125 wt % Co and 0.0125 wt % Mn with regard to solid binder.

Curing with **2** only takes place upon continued exposure of the film of paint to light, and samples held in the dark fail to undergo curing. Notably, films held in the dark for 18 or 24 h cured in the same time once exposed to light (Figure S3).[27] These results contrast with those obtained with **3** (CoNeo) and **4** (Mn/MeTACN), which undergo curing in the dark at a rate similar to that under light.

From here, for kinetic and mechanistic studies, only paints dosed with **2** will be discussed further.

Time-resolved FTIR and Raman spectroscopies show the same spectral changes of the alkyd paint matrix during curing of Setal-270 dosed with **2** as with the Co- and Mn-based reference catalysts **3** and **4**. Consumption of *cis*-alkene (3008 cm^{-1}) and formation of (conjugated) *trans*-alkene (987 cm^{-1}) as well as a hydroxylated species (3400 cm^{-1}) is observed by FTIR spectroscopy,[33] and consumption of C═C bonds (1656, 1265 cm^{-1}) is observed by Raman spectroscopy (Figure 3 and Figures S11 and S24).[44]

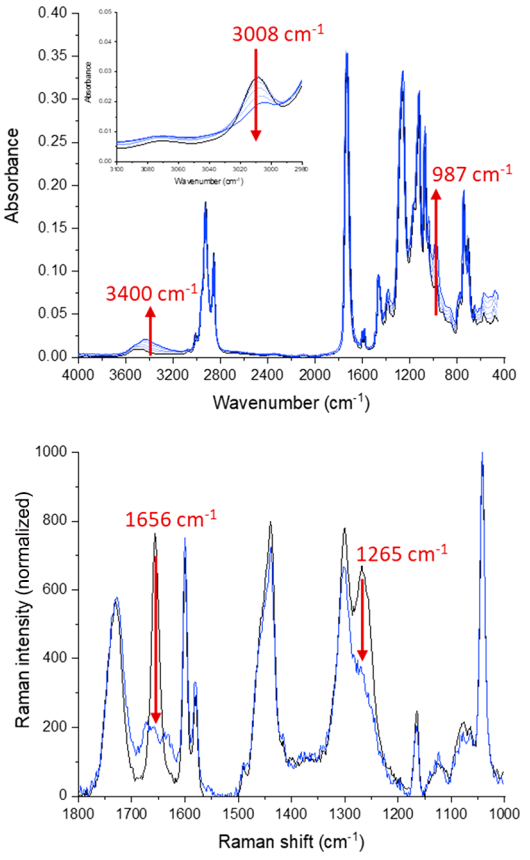

Figure 3. FTIR (top) and Raman (bottom) spectra showing curing of Setal-270 dosed with [(Cp)Fe(Ch)] (**2**) at 0.10 wt %.

https://doi.org/10.1021/jacsau.1c00579
JACS Au 2022, 2, 531−540

These changes in double bond and the formation of hydroxylated species are an indication of reactivity but, on their own, not proof of cross-linking. However, loss of conjugation by other mechanisms, such as oxidation, would lead to poor film performance. Furthermore, spin-trapping experiments have shown the presence of C- and O-based (conjugated) fatty acid radicals characteristic for radical-based cross-linking (vide infra). In other words, alkyd curing using the new Fe catalyst involves a radical (hydroperoxide-based) cross-linking process, similar to the curing process mediated by cobalt driers (Scheme 1).

Dependence of Latency and Curing on Light

The impact of the primary inner filter effect on the efficiency of photoactivation and drying rates through the films was probed by UV/vis absorption spectroscopy. Regardless of the applied concentrations (0.0−0.14 wt % Fe), 90 μm thick films show ∼98−99% transmission in the visible region, and hence, light transmission is not a limiting factor for photoactivation (Figure S10).

The 90 μm thin films of Setal-270 dosed with 0.10 wt % **2** were exposed to a short flash of broad band irradiation either once or several times. The samples were left in the dark for 30 min after each flash and characterized by FTIR spectroscopy, with the conversion of the starting material manifested in a decrease in the band at 3008 cm^{-1} (*cis*-C**═**C**−**H) characteristic for the unsaturated fatty acids.[33] Neither a single nor repeated flashes led to significant conversion, just as for control samples kept in the dark for the same periods (Figure S12).

Thin films, which were held in the dark and then exposed to light for 30 min periodically, showed significantly more conversion during the periods of illumination (Figure 4).

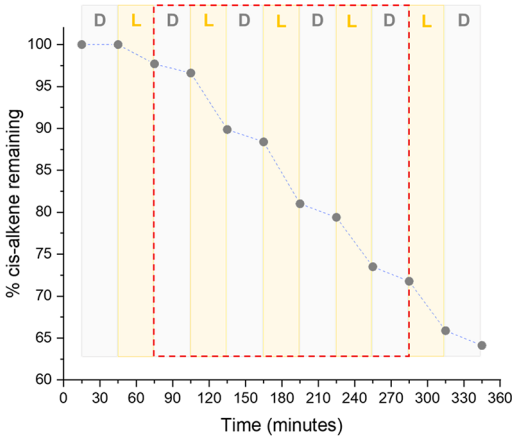

Figure 4. Switching between 30 min periods of dark (D) and light (L) shows a strong dependence of conversion on light and hence the necessity for continuous irradiation, most apparent in the highlighted central area.

Films exposed to light continuously show an immediate and strong slowdown of conversion once the samples were placed in the dark compared to samples kept under illumination (Figure S17).

As conversion in the dark was minor, it seems likely that the species formed after photoactivation decay into one or more species of low activity. The results further indicate that catalyst activation is a gradual process and that continuous irradiation is required to maintain a steady-state concentration of the active species and thereby a stable curing rate over the entire drying period. This model rationalizes the decrease in conversion in the dark after periods of illumination,[27] as well as the excellent latency and skin-free storage of paint formulations with complex **2** as the catalyst in a regular metal paint can.

In fact, a sample stored for ∼2 months showed little difference in conversion rate to a freshly prepared sample, and samples stored for ∼9.5 and ∼12.5 months still showed excellent curing behavior (Figure S13).

Photolysis of the Cationic Complex

Photolysis of $[(Cp)Fe(arene)](PF_6)$ complexes in acetonitrile leads to formation of $[(Cp)Fe(NCCH_3)_3]^+$, which is not stable at room temperature and undergoes ligand exchange to form ferrocene and $[Fe(NCMe)_6](PF_6)_2$.[34] A degassed solution of **1** in acetonitrile-d_3 under ambient laboratory light showed an exponential decrease in absorbance, as expected for a photochemical displacement reaction, with a close to linear decay in the first 7 h, with simultaneous formation of ferrocene being observed (Figure S4).

Photolysis in Setal-270 also showed a linear release of C_6H_6 over 6 h (Figures 5 and S6). However, here, formation of

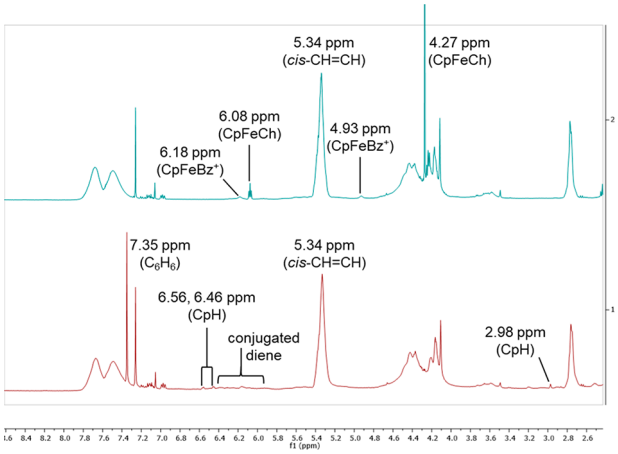

Figure 5. ^{1}H NMR spectrum (top) of **2** in degassed Setal-270 prepared under N_2 and (bottom) after exposure to air and light.

ferrocene was not observed, and only minor amounts of cyclopentadiene (CpH) were formed, showing that the Cp ligand remains mostly bound to iron after photoactivation in the alkyd matrix.

Irradiation of **1** in a frozen tetrahydrofuran glass under anaerobic conditions in the cavity of an electron paramagnetic resonance (EPR) spectrometer resulted in an EPR signal characteristic for an $S = 2$ (high-spin) Fe^{II} species (Figure S28), most likely a $[(Cp)Fe(S)]^+$ species (S = solvent), in line with previous reports of an $S = 2$ spin state for (coordinatively unsaturated) mono-$CpFe^{II}$ complexes.[35]

Freshly dried paint samples (after 1 day of curing) reveal similar (but not identical) $S = 2$ signals, together with smaller amounts of $S = 5/2$ signals characteristic for high-spin Fe^{III} ions present in Fe_2O_3 nanoparticles. A major part of the (detectable) iron species present in these freshly prepared samples thus seem to be in the high-spin Fe^{II} configuration (Figure S27).

The combined NMR and EPR data thus suggest that, during paint curing, high-spin $[(Cp)Fe(L)]^+$ (L = alkyd donor) species are formed, and the dependence of curing on their continued formation indicates that these species are responsible for the aerobic paint curing process. We speculate that in the (freshly)

https://doi.org/10.1021/jacsau.1c00579
JACS Au 2022, 2, 531−540

cured paint samples these species are most likely trapped in a poorly active form, presumably bound to carboxylates or other donors in the alkyd matrix or by the formation of μ-oxo (Fe^{III}) dimers (antiferromagnetic coupling between the spins on Fe in such dimers might preclude their EPR detection).

Over several days, the color of the cured films turns (light) orange, which is an indication of (further) oxidation to Fe^{III} and possibly clustering, with the color being caused by an $Fe^{III} \leftarrow O$ ligand to metal charge transfer band. In fact, the Fe^{II} $S = 2$ EPR signals disappear over time, and in older dried paint samples, only the $S = 5/2$ signals characteristic for Fe_2O_3 remain (in increased intensity; Figure S29).

Based on the strength of Fe^{III}-phosphonate bonds,[36] we considered that addition of an (alkyl)phosphonic acid might prevent the formation of these colored species. Indeed, addition of 1 molar equiv of *n*-octylphosphonic acid led to much less coloration. We are currently investigating this effect.

Kinetics of Curing

The onset of curing, as well as the continuation of the radical process, was monitored through the conversion of *cis*-alkene by FTIR spectroscopy (3008 cm^{-1}, *cis*-C=C−H).[33] In the curing of 90 μm films dosed with the reference Co- and Mn-based catalysts CoNeo (**3**) and Mn/MeTACN (**4**) (both dosed with 2-butanone oxime), an induction period of 50−60 min was observed. After this first hour, conversion starts and accelerates in the following 60−90 min, which is indicative of a burst in formation of free radical species involved in a radical-chain autoxidation process (Figure 6).

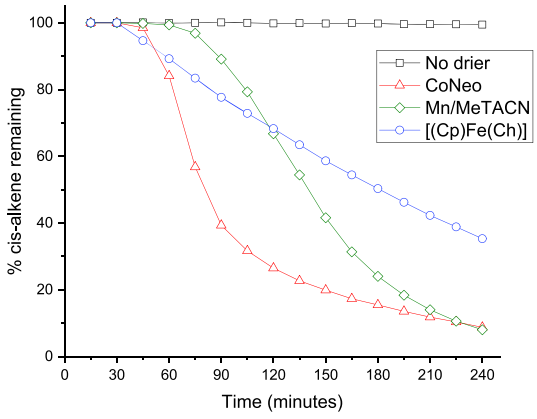

Figure 6. Conversion of *cis*-alkene in Setal-270 for three catalysts followed by decrease in absorbance at 3008 cm^{-1}.

The $[(Cp)Fe(Ch)]/[(Cp)Fe(C_6H_6)]^+$ system shows completely different curing kinetics. Conversion shows a weak exponential, near-linear decrease of the concentration of the *cis*-alkene (see Figure 6), coinciding with the near-linear rate of photoinduced loss of C_6H_6 from $[(Cp)Fe(C_6H_6)]^+$ in Setal-270 (Figure S6).

Despite the higher residual *cis*-alkene content (~40%) for **2** (dosed at 0.10 wt %) after 4 h, in comparison to that for paints dosed with **3** and **4** (~10%), all films had cured within the 4 h of the experiment. This result shows that the rate (and degree) of C=C conversion not necessarily translates 1:1 to the curing time. Experiments using $Mn(acac)_3$ and $VO(neodecanoate)_2$ had previously also shown a similar behavior.[37] Over several hours more, films with **2** also reach 90% conversion, showing an overall exponential decrease of the concentration of *cis*-alkene (Figure S17).

Combined with the studies under irradiation (e.g., Figure 4), the linear consumption of alkene, apparent from Figure 6, probably arises from continuous generation of new active species (most likely $[(Cp)Fe(L)]^+$, L = alkyd donor based on the EPR studies) by irradiation of $[(Cp)Fe(arene)]^+$. We speculate that the activity of these species decreases rapidly, perhaps because of a fast $Fe^{II} \rightarrow Fe^{III}$ oxidation, resulting in a steady-state concentration of active iron species during curing.

Interestingly, the dependence of the curing rate on the concentration of **2** (Figure S15) shows a broken order in [Fe] (rate = $k_{obs}[Fe]^{0.5}$). This implies that a dinuclear iron complex, such as $[(Cp)Fe(\mu\text{-}L)Fe(Cp)]$ (μ-L = bridging ligand, e.g., ester or carboxylate) or $[(Cp)Fe(\mu\text{-}O_2)Fe(Cp)]$, is formed, which breaks up into active mononuclear species before the rate-limiting step(s) involved in aerobic paint curing. However, the overall kinetics of this system are complex, and a interplay between the elementary steps of paint curing, O_2 diffusion, and the rate of the photoactivation process cannot be excluded.

Radical Mechanism and O_2 Consumption

To probe the (radical) mechanism of alkyd curing using the $[(Cp)Fe(Ch)]/[(Cp)Fe(arene)]^+$ system, spin-trapping experiments were performed using phenyl-*N*-*tert*-butylnitrone (PBN) and 5,5-dimethyl-1-pyrrolidine-*N*-oxide (DMPO). Control experiments without **2** showed a very weak EPR signal for samples prepared under air or in a N_2-filled glovebox, which increased slightly over ~2 h under ambient lighting.

Samples dosed with **2** showed the same spectral features but with a markedly increased intensity. In the case of PBN, a distinction could not be made between the radicals trapped under N_2 or air atmosphere (Figure S30). Fitting of the DMPO spectra revealed that C-centered radicals (a_N = 14.25 G, a_H = 20.88 G) are trapped for the sample under N_2, whereas O-centered radicals (a_N = 12.99 G, a_H = 6.66 G) are trapped for the sample under aerobic conditions (Figure S30). These trapped species originate from a conjugated fatty acid diene radical and a conjugated diene alkoxyl radical, respectively.[38]

These results can be rationalized by slow formation of peroxides during storage of the alkyd, which undergo Fe-catalyzed cleavage, with the active catalyst being generated upon photolysis of $[(Cp)Fe(arene)]^+$. In the absence of Fe, only minor radical formation is observed upon exposing the paint samples to light. Under an N_2 atmosphere, the radicals formed likely abstract a hydrogen atom at a bisallylic position of the abundantly available polyunsaturated alkenes, forming stabilized C-centered radicals which are subsequently trapped by PBN/DMPO. Under air, the C-centered radicals rapidly react with O_2 to form peroxyl radicals (see Scheme 1) before they are trapped by PBN/DMPO. The observation that the alkoxyl radical adduct is formed under air is in line with previous findings that (attempted) spin-trapping of the (conjugated) fatty acid peroxyl radical by DMPO at room temperature leads to the formation of the alkoxyl radical instead.[39]

Oxygen consumption by wet paint in a closed flask (1 mL paint, 15 mL air) was followed with both a pressure sensor and O_2 detector. This revealed a concomitant pressure decrease at a constant rate initially (~1−2 h), but over longer periods (~6 h), the pressure decrease proved to be exponential (Figure S21). With various O_2 concentrations (using air/N_2 mixtures), in each case a linear decrease was observed over ~60 min; furthermore, from these kinetic experiments, a broken order in $[O_2]$ of ~0.6 was determined (Figure S22).

https://doi.org/10.1021/jacsau.1c00579
JACS Au 2022, 2, 531−540

When varying the light intensity using blue LED strips as the light source, we observed a correlation between light intensity and oxygen consumption (Figure S23). Similarly, when following the *cis*-alkene consumption of 90 μm films by FTIR spectroscopy, we also observed a correlation between light intensity and alkene consumption (Figure S19). FTIR spectral data indicate an order of 0.5 in [Fe] (rate = k_{obs}[Fe]$^{0.5}$) for all four light intensities studied (Figure S19), consistent with the experiments performed under ambient lighting (Figure S15).

Hardness Development and Confocal Raman Microscopy

In addition to decreasing the drying time, new catalysts should also provide a hard coating. Hardness development of coatings dried using **2**, **3**, and **4** was assessed using a pendulum damping test, where the number of oscillations needed to reduce from an initial deflection of 6 to 3° was measured.

Films prepared using [(Cp)Fe(Ch)] (**2**) show a hardness increase comparable to coatings cured with CoNeo (**3**). Coatings cured with Mn/MeTACN (**4**) do not show this (see Table 1 and Table S1 in the Supporting Information); in fact, softer coatings are a common drawback of known cobalt-free catalysts.[16] Although very hard coatings may become brittle over time, we did not observe this for coatings cured with **2**. To the best of our knowledge, this is the first iron-based catalyst that combines latency with good drying times and hardness values comparable to those of cobalt catalysts.

Table 1. Hardness Values (Number of Oscillations, Average of Duplicate) for 90 μm Paint Films, Using the König Pendulum Test

time[a]	Co (**3**)	Mn (**4**)	Fe (**2**)[b]	Fe (**2**)[c]
1 day	15	13	13	14
4 days	21.5	13	16	18.5
7 days	24.5	13	18.5	21.5
14 days	29.5	13	21.5	26.5
100 h at 50 °C[d]	40	15	30.5	38.5

[a]The samples were stored at 23 °C and 50% relative humidity. [b]Dosed at 0.10 wt % Fe. [c]Dosed at 0.20 wt % Fe. [d]Samples were kept at 50 °C for 100 h after 14 days at initial conditions.

Previous studies with solid-state NMR spectroscopy suggested that the hardness increase over time with cobalt-based catalysts is due to a "front-forming" mode of curing. With **3**, a solid film forms on top of the coating, with hardening developing through the film as the curing progresses (front-forming curing), whereas for **4**, there is no such difference between the top and bulk of the coating (homogeneous curing).[40] A depth profile study using confocal Raman microscopy revealed for **3** that alkene conversion (1656 cm^{-1} band) at the top of the film was indeed faster than deeper in the film, while such a strong depth dependence was not observed when using **4**.[41] Due to the correspondence of the results from solid-state NMR spectroscopy and confocal Raman microscopy, the disappearance of double bonds was directly connected to the formation of cross-links, and hence, the authors concluded that front-forming curing leads to a cross-linking density intrinsically higher than that of homogeneous curing.[42] However, based on the results obtained with the new Fe-based catalyst **2**, we now come to a different conclusion.

Raman spectra recorded during curing with CoNeo (**3**) and Mn/MeTACN (**4**) show an initial increase in Raman scattering at 1656 cm^{-1}, followed by a gradual decrease (Figure S25). The initial increase at 1656 cm^{-1} is due to formation of a conjugated diene (with an intrinsically higher Raman scattering cross section) from the linoleic and linolenic nonconjugated dienes,[43,44] which occurs upon hydroperoxide formation in the initiation and propagation steps of alkyd curing (Scheme 1). This behavior was not reported in the previous study by Oyman et al.[41]

The results from our depth profile studies using confocal Raman microscopy are in accordance with literature, showing front-forming curing for CoNeo (**3**) and homogeneous curing for Mn/MeTACN (**4**). For the new [(Cp)Fe(Ch)]/[(Cp)Fe(arene)]$^+$ system, we do not observe a depth dependence of the curing process (i.e., homogeneous curing), as observed for **4** (Figure S26). As the paint layers dosed with [(Cp)Fe(Ch)] (**2**) can reach much higher hardness values than those dosed with **4**, the assumption that front-forming curing leads to harder paint layers, while homogeneous curing leads to softer materials is incorrect or at least not generally applicable.

A possible explanation for the hardness development of paints cured with the [(Cp)Fe(Ch)]/[(Cp)Fe(arene)]$^+$ system is that the slow release of active iron continues even after the coating feels dry, resulting in continuous photoinduced formation of active species during the continued curing process. These species presumably migrate through the cured coating, leading to more cross-links despite the homogeneous curing process. Ring opening of epoxides formed during the curing[11] by photoactivated [(Cp)Fe(arene)]$^+$ could also lead to additional cross-links.[26]

Another possible explanation for the observed differences in hardness could be that the Co and Fe catalysts cause less oxidation-induced degradation (thus producing fewer small molecules acting as plasticizers) than the Mn catalyst, as oxidation has been shown to be linked to degradation in oil paintings.[45] Indeed, PBN/DMPO spin-trapping experiments in alkyd with **2** (Figure S30) and NMR studies of air oxidation of methyl linoleate catalyzed by **1** (Figures S8 and S9) revealed remarkably clean reactions. The possibility of oxidation-induced plasticizer formation having an influence on the different hardness values obtained with different catalysts will be investigated in a follow-up study.

CONCLUSIONS

We have shown that the [(Cp)Fe(Ch)]/[(Cp)Fe(arene)]$^+$ system functions as a (photo)latent catalyst for the curing of alkyd coatings, performing equally well as the reference systems CoNeo (**3**) and Mn/MeTACn (**4**) in terms of drying time and outperforming **4** in terms of hardness development, without the need for 2-butanone oxime as a blocking agent. The newly identified catalyst is the first system based on an abundant and nontoxic transition metal (Fe) that combines good drying and hardness values without the need for an antiskinning agent.

Based on the light−activity studies, we conclude that photolysis leads to the formation of short-lived active species, explaining the excellent latency. EPR studies suggest that high-spin [(Cp)Fe^{II}(L)]$^+$ species, photogenerated from [(Cp)-Fe^{II}(arene)]$^+$, are involved in the curing process.

Further studies into the activation, hardness development, and color development (and the prevention thereof) of alkyd curing using [(Cp)Fe(Ch)]/[(Cp)Fe(arene)]$^+$ are currently underway in our group, including complexes based on nonvolatile arenes, and we see a bright future for photochemically derived latency in the (peroxide-based) cross-linking of coatings.

https://doi.org/10.1021/jacsau.1c00579
JACS Au 2022, 2, 531−540

EXPERIMENTAL SECTION

Synthesis of the Fe Complexes

Iron complexes [(Cp)Fe(C_6H_6)](PF_6) (**1**), [(Cp)Fe(C_6H_6Me)](PF_6) (**1′**), [(Cp)Fe(Ch)] (**2**), and [(Cp)Fe(Ch′)] (**2′**) were synthesized following modified literature procedures (see the Supporting Information).

Coating Formulations

The alkyd solution Setal-270 SM-70 was obtained from Allnex (formerly Nuplex Resins). It is an alkyd solution based on soybean oil containing 70 wt % solids, the remainder being hydrotreated naphtha; the 70 wt % alkyd resin itself is produced from soybean oil (65% by mass), phthalic anhydride (25% by mass), and pentaerythritol (10% by mass). For a 0.10 wt % dosage of [(Cp)Fe(Ch)] (**2**) (wt % metal with regard to solids), an amber vial containing 7.90 g of Setal-270 and a small spatula was placed on the balance and tared. Afterward, 19.8 mg of [(Cp)Fe(Ch)] (**2**) dissolved in heptane was added; the mixture was stirred with a spatula, and heptane was added to a mass of 2.10 g (total mass = 7.90 + 2.10 = 10.00 g), after which it was stirred with a spatula and stored in the dark. Similarly, for a 0.05 wt % dosage of [(Cp)Fe(C_6H_6)](PF_6) (**1**), 17.1 mg of **1** dissolved in acetone was added to 7.90 g of Setal-270, with additional acetone added to a mass of 2.10 g. The paint mixtures were left standing overnight at room temperature before they were applied for measurements.

Drying Time Measurements

Drying times were determined according to ASTM D5895-13 using a BK recorder (wet film thickness 90 μm). After the application of the film on a glass panel (300 × 25 mm), a vertical blunt needle, pressed upon by a 5 g load, was placed into the freshly applied film and then dragged in a straight line through the drying paint in the longitudinal direction of the panel. The so-called "dry-hard time", that is, when drying has proceeded sufficiently that the paint film is not displaced anymore (stage III of drying in ASTM D5895-13), was determined in this way.

NMR and EPR Spectroscopy

NMR spectra were recorded on a Bruker AMX 400 spectrometer at room temperature. X-band EPR spectra (room temperature and 20 K) were recorded on a Bruker EMX-Plus CW X-band EPR spectrometer equipped with an ER 4112HV-CF100 He cryostat.

UV/Vis Spectroscopy

UV/vis spectra were recorded on a double-beam Shimadzu UV-2600 spectrometer. Paints were prepared on 10 g scale using 7.90 g of Setal-270. Absorption measurements of the paints were performed in 1.0 cm quartz cuvettes or as 90 μm wet films on glass slides.

FTIR Spectroscopy

FTIR spectra were recorded to follow the spectral changes taking place during the curing of Setal-270 with either the commercial driers CoNeo (**3**) and Mn/MeTACN (**4**) or the [(Cp)Fe(Ch)]/[(Cp)Fe(C_6H_6)]$^+$ system. For attenuated total reflectance (ATR)-IR measurements, using a Spectrum Two FTIR spectrometer (ATR mode, PerkinElmer) equipped with an UATR accessory, a 90 μm thin film was applied on the ATR crystal using a film applicator, and a spectrum was recorded at 15 min intervals during 6 h. Each spectrum was recorded using 16 scans with a spectral resolution of 4 cm^{-1} in the spectral range of 450−4000 cm^{-1}.

Raman Spectroscopy

Raman spectra at 785 nm were recorded to determine the spectral changes taking place during the curing of Setal-270 with either the commercial driers CoNeo (**3**) and Mn/MeTACN (**4**) or the [(Cp)Fe(Ch)]/[(Cp)Fe(C_6H_6)]$^+$ system. Raman spectra at 785 nm were recorded with either a RamanFlex instrument (PerkinElmer) equipped with an Inphotonics industrial probe or with a home-built Raman microscope (BX51) equipped with a free space laser (75 mW, Ondax, with a 785 nm laser line clean-up filter) and dichroic mirror to bring the laser collinear with the optical axis of the microscope. The Raman scattering was collected in backscattering (180°) mode with a Thorlabs fiber launch and round to line bundle of 50 μm fiber-optic cable to a Shamrock 163 spectrograph (ANDOR Technology) and dispersed onto a iDUS-420-BUEX2 CCD camera. Spectra were calibrated with polystyrene. Samples (90 μm thin films) had cured for 5 days before Raman analysis. The spectra were obtained using 10 acquisitions of 5 s exposure time for every spectrum. A reference spectrum of Setal-270 was obtained by recording a spectrum after applying a drop of Setal-270 in heptane on a glass plate. A linear baseline correction (1000−1800 cm^{-1} area) was performed, and the spectra were normalized to the arene band at 1032 cm^{-1}.

Oxygen Consumption Measurements

Oxygen consumption by wet paint was followed with both a pressure sensor (Man on the Moon, X102-A08 kit, Universidad Zaragoza) and an optical oxygen meter (FireSting, probe XC7-548-208; see Figure S20 in the Supporting Information). Measurements were performed in a closed, tube-shaped flask (1 mL paint, 15 mL air) by leveling the wet paint over the long side of the flask before starting the measurements. The oxygen concentration was measured once every 60 s, and the pressure was measured once every 10 s. The measurements were performed using a lightbox setup (see Figure S16 in the Supporting Information).

ASSOCIATED CONTENT

Supporting Information

The Supporting Information is available free of charge at https://pubs.acs.org/doi/10.1021/jacsau.1c00579.

Synthetic procedures, materials and methods, and supporting figures (PDF)

AUTHOR INFORMATION

Corresponding Author

Bas de Bruin − *Homogeneous, Supramolecular and Bio-Inspired Catalysis Group, Van 't Hoff Institute for Molecular Sciences, University of Amsterdam, 1098 XH Amsterdam, The Netherlands*; orcid.org/0000-0002-3482-7669; Email: b.debruin@uva.nl

Authors

Johan Bootsma − *Homogeneous, Supramolecular and Bio-Inspired Catalysis Group, Van 't Hoff Institute for Molecular Sciences, University of Amsterdam, 1098 XH Amsterdam, The Netherlands*

Wesley R. Browne − *Molecular Inorganic Chemistry group, Stratingh Institute for Chemistry, University of Groningen, 9747 AG Groningen, The Netherlands*; orcid.org/0000-0001-5063-6961

Jitte Flapper − *Akzo Nobel Decorative Coatings B.V., 2171 AJ Sassenheim, The Netherlands*

Complete contact information is available at: https://pubs.acs.org/10.1021/jacsau.1c00579

Funding

This work is part of the Advanced Research Center for Chemical Building Blocks, ARC CBBC (project 2016.001.UvA), which is cofounded and cofinanced by The Netherlands Organization for Scientific Research (NWO, contract 736.000.000) and The Netherlands Ministry of Economic Affairs and Climate.

Notes

The authors declare the following competing financial interest(s): J.B., J.F. and B.B. are inventors on PCT International Patent Application WO2021/001410 (to Akzo Nobel Coatings

International B.V.), which claims the use of catalysts described in this work.

■ ACKNOWLEDGMENTS

Henk Kelders (AkzoNobel) and Zhi Qhi Hu (AkzoNobel) are thanked for their help with the BK drying time and König hardness value measurements. Felix de Zwart (University of Amsterdam) is thanked for fruitful discussions, in particular, with regard to the initial EPR studies. Tijmen Bakker (University of Amsterdam) is thanked for assistance with the LED characterization.

■ REFERENCES

(1) (a) Lüning, Ü. Switchable Catalysis. *Angew. Chem., Int. Ed.* **2012**, *51*, 8163−8165. (b) Leibfarth, F. A.; Mattson, K. M.; Fors, B. P.; Collins, H. A.; Hawker, C. J. External Regulation of Controlled Polymerizations. *Angew. Chem., Int. Ed.* **2013**, *52*, 199−210. (c) Chirila, A.; Gopal Das, B.; Kuijpers, P. F.; Sinha, V.; de Bruin, B. Application of Stimuli Responsive and 'Non-innocent' Ligands in Base Metal Catalysis. In *Non-Noble Metal Catalysis: Molecular Approaches and Reactions*; Klein Gebbink, R. J., Moret, M.-E., Eds.; Wiley Press, 2019; Chapter 1, pp 1−31, ISBN 978-3-527-69908-7.

(2) Blanco, V.; Leigh, D. A.; Marcos, V. Artificial Switchable Catalysts. *Chem. Soc. Rev.* **2015**, *44*, 5341−5370.

(3) (a) Stoll, R. S.; Hecht, S. Artificial Light-Gated Catalyst Systems. *Angew. Chem., Int. Ed.* **2010**, *49*, 5054−5075. (b) Neilson, B. M.; Bielawski, C. W. Illuminating Photoswitchable Catalysis. *ACS Catal.* **2013**, *3*, 1874−1885.

(4) Lai, H.; Zhang, J.; Xing, F.; Xiao, P. Recent Advances in Light-Regulated Non-Radical Polymerizations. *Chem. Soc. Rev.* **2020**, *49*, 1867−1886.

(5) (a) Corrigan, N.; Yeow, J.; Judzewitsch, P.; Xu, J.; Boyer, C. Seeing the Light: Advancing Materials Chemistry Through Photopolymerization. *Angew. Chem., Int. Ed.* **2019**, *58*, 5170−5189. (b) Pan, X.; Tasdelen, M. A.; Laun, J.; Junkers, T.; Yagci, Y.; Matyjaszewski, K. Photomediated Controlled Radical Polymerization. *Prog. Polym. Sci.* **2016**, *62*, 73−125. (c) Chen, M.; Zhong, M.; Johnson, J. A. Light-Controlled Radical Polymerizations: Mechanisms, Methods, and Applications. *Chem. Rev.* **2016**, *116*, 10167−10211.

(6) (a) Corrigan, N.; Shanmugam, S.; Xu, J.; Boyer, C. Photocatalysis in Organic and Polymer Synthesis. *Chem. Soc. Rev.* **2016**, *45*, 6165−6212. (b) Zivic, N.; Bouzrati-Zerelli, M.; Kermagoret, A.; Dumur, F.; Fouassier, J.-P.; Gigmes, D.; Lalevée, J. Photocatalysts in Polymerization Reactions. *ChemCatChem.* **2016**, *8*, 1617−1631.

(7) (a) Lepage, M. L.; Simhadri, C.; Liu, C.; Takaffoli, M.; Bi, L.; Crawford, B.; Milani, A. S.; Wulff, J. E. A Broadly Applicable Cross-Linker for Aliphatic Polymers Containing C-H Bonds. *Science* **2019**, *366*, 875−878. (b) de Zwart, F. J.; Bootsma, J.; de Bruin, B. Cross-Linking Polyethylene Through Carbenes. *Science* **2019**, *366*, 800.

(8) Hofland, A. Alkyd Resins: from Down and Out to Alive and Kicking. *Prog. Org. Coat.* **2012**, *73*, 274−282.

(9) Soucek, M. D.; Khattab, T.; Wu, J. Review of Autoxidation and Driers. *Prog. Org. Coat.* **2012**, *73*, 435−454.

(10) Muizebelt, W. J.; Nielen, M. W. F. Oxidative Crosslinking of Unsaturated Fatty Acids Studied with Mass Spectrometry. *J. Mass Spectrom.* **1996**, *31*, 545−554.

(11) van Gorkum, R.; Bouwman, E. The Oxidative Drying of Alkyd Paint Catalysed by Metal Complexes. *Coordin. Chem. Rev.* **2005**, *249*, 1709−1728.

(12) Honzíček, J. Curing of Air-Drying Paints: A Critical Review. *Ind. Eng. Chem. Res.* **2019**, *58*, 12485−12505.

(13) Erich, S. J. F.; Gezici-Koç, Ö.; Michel, M.-E. B.; Thomas, C. A. A. M.; van der Ven, L. G. J.; Huinink, H. P.; Flapper, J.; Duivenvoorde, F. L.; Adan, O. C. G. The Influence of Calcium and Zirconium Based Secondary Driers on Drying Solvent Borne Alkyd Coatings. *Polymer* **2017**, *121*, 262−273.

(14) European Commission; https://ec.europa.eu/environment/chemicals/reach/reach_en.htm (accessed 2021-04-30).

(15) Chardon, F.; Denis, M.; Negrell, C.; Caillol, S. Hybrid Alkyds, the Glowing Route to Reach Cutting-Edge Properties? *Prog. Org. Coat.* **2021**, *151*, 106025.

(16) Hage, R.; de Boer, J. W.; Maaijen, K. Manganese and Iron Catalysts in Alkyd Paints and Coatings. *Inorganics* **2016**, *4*, 11.

(17) Simpson, N.; Maaijen, K.; Roelofsen, Y.; Hage, R. The Evolution of Catalysis for Alkyd Coatings: Responding to Impending Cobalt Reclassification with Very Active Iron and Manganese. *Catalysts, Using Polydentate Nitrogen Donor Ligands. Catalysts* **2019**, *9*, 825.

(18) Hage, R.; de Boer, J. W.; Gaulard, F.; Maaijen, K. Manganese and Iron Bleaching and Oxidation Catalysis. In *Advances in Inorganic Chemistry*; van Eldik, R., Hubbard, C. D., Eds.; Academic Press, 2013; Chapter 3, Vol. *65*, pp 85−116, ISBN: 978-0-12-404582-8.

(19) (a) Kalenda, P.; Holeček, J.; Veselý, D.; Erben, M. Influence of Methyl Groups on Ferrocene on Rate of Drying of Oxidizable Paints by using Model Compounds. *Prog. Org. Coat.* **2006**, *56*, 111−113. (b) Stava, V.; Erben, M.; Vesely, D.; Kalenda, P. Properties of Metallocene Complexes During the Oxidative Crosslinking of Air Drying Coatings. *J. Phys. Chem. Solids* **2007**, *68*, 799−802. (c) Erben, M.; Veselý, D.; Vinklárek, J.; Honzíček, J. Acyl-Substituted Ferrocenes as Driers for Solvent-Borne Alkyd Paints. *J. Mol. Catal. A: Chem.* **2012**, *353-354*, 13−21.

(20) (a) Honzíček, J.; Vinklárek, J. Chemical Curing of Alkyd Resin Catalyzed by Benzoylferrocene: Performance, Kinetics, and Thickness Effects. *J. Appl. Polym. Chem.* **2018**, *135*, 46184. (b) Honzíček, J.; Fedorova, T.; Vinklárek, J.; Mikysek, T.; Císařová, I. Modified Ferrocenes as Primary Driers for Formulations of Alkyd Coatings. *Coatings* **2020**, *10*, 873.

(21) Salata, R. R.; Pellegrene, B.; Soucek, M. D. Visible Light Cure Packages for Improved Drying Kinetics in Alkyd Coatings. *Prog. Org. Coat.* **2020**, *144*, 105672.

(22) Zhou, H.; Song, D.; Zhong, C.; Ye, G. Theoretical and Experimental Study of Light-assisted Polymerization by Multi-mechanistic Action. *Sci. Rep.* **2016**, *6*, 38473.

(23) Ye, G.; Courtecuisse, F.; Allonas, X.; Ley, C.; Croutxe-Barghorn, C.; Raja, P.; Taylor, P.; Bescond, G. Photoassisted Oxypolymerization of Alkyd Resins: Kinetics and Mechanisms. *Prog. Org. Coat.* **2012**, *73*, 366−373.

(24) Hubert, J. C.; Venderbosch, R. A. M.; Muizebelt, W. J.; Klaasen, R. P.; Zabel, K. H. Singlet Oxygen Drying of Alkyd Resins and Model Compounds. *J. Coat. Technol.* **1997**, *69*, 59−64.

(25) Astruc, D. Organo-Iron Complexes of Aromatic Compounds. Applications in Synthesis. *Tetrahedron* **1983**, *39*, 4027−4095.

(26) Lohse, F.; Zweifel, H. Photocrosslinking of Epoxy Resins. In *Epoxy Resins and Composites III. Advances in Polymer Science*; Dušek, K., Ed.; Springer: Berlin, 1986; Chapter 10, pp 61−81, ISBN 978-3-540-15936-0.

(27) Solvent-borne alkyd paints (e.g., Setal-270) are typically used outside or in (well-ventilated and) well-illuminated rooms, and normally, there is enough light. Even if not, the experiments in this paper show that the catalyst can stay dormant until there is sufficient light. Also, (through-)curing takes place in the shade, although obviously slower than in the light (see Figure S17).

(28) Jones, D.; Pratt, L.; Wilkinson, G. π-Cyclohexadienyl Compounds of Manganese, Rhenium, Iron, and Ruthenium. *J. Chem. Soc.* **1962**, *0*, 4458−4463.

(29) Brown, R. A.; Houlton, A.; Roberts, R. M. G.; Silver, J.; Slade, E. Studies of the Bonding in Iron(II) Cyclopentadienyl and Arene Sandwich Compounds. Part 3. Carbon-13 Nuclear Magnetic Resonance and Iron-57 Mössbauer Spectroscopic Studies on [(η-cyclohexadienyl)(η-cyclopentadienyl)]iron(II) Complexes. *J. Chem. Soc., Dalton Trans.* **1993**, 1519−1523.

(30) Sutherland, R. G.; Zhang, C. H.; Chowdhury, R. L.; Píorko, A.; Lee, C. C. Product Distributions in the Addition of the Hydride Ion to Cyclopentadienyliron Complexes of Substituted Benzenes. *J. Organomet. Chem.* **1987**, *333*, 367−381.

https://doi.org/10.1021/jacsau.1c00579
JACS Au 2022, 2, 531−540

(31) Nesmeyanov, A. N.; Vol'kenau, N. A.; Shilovtseva, L. S.; Petrakova, V. A. The Reactivity of Cyclohexadienyl(Cyclopentadienyl) Iron Derivatives. *J. Organomet. Chem.* **1975**, *85*, 365−373.
(32) McNair, A. M.; Schrenk, J. L.; Mann, K. R. Effect of Arene Substituents and Temperature on the Arene Replacement Reactions of $[(\eta^5\text{-}C_5H_5)Fe(\eta^6\text{-arene})]^+$ and $[(\eta^5\text{-}C_5H_5)Fe(\eta^6\text{-arene})]^+$. *Inorg. Chem.* **1984**, *23*, 2633−2640.
(33) van de Voort, F. R.; Ismail, A. A.; Sedman, J.; Emo, G. Monitoring the Oxidation of Edible Oils by Fourier Transform Infrared Spectroscopy. *J. Am. Oil. Chem. Soc.* **1994**, *71*, 243−253.
(34) Gill, T. P.; Mann, K. R. Photochemistry of $[(\eta\text{-}C_5H_5)Fe(\eta\text{-}p\text{-xyl})]PF_6$ in Acetonitrile Solution. Characterization and Reactivity of $[(C_5H_5)Fe(CH_3CN)_3]^+$. *Inorg. Chem.* **1983**, *22*, 1986−1991.
(35) (a) Reiners, M.; Maekawa, M.; Baabe, D.; Zaretzke, M.-K.; Schweyen, P.; Daniliuc, C. G.; Freytag, M.; Rader, J.; Hohenberger, J.; Sutter, J.; Meyer, K.; Walter, M. D. Monomeric Fe(III) Half-Sandwich Complexes $[Cp'FeX_2]$ − Synthesis, Properties and Electronic Structure. *Dalton Trans.* **2018**, *47*, 10517−10526. (b) Gro*β*, O. A.; Lauk, S.; Müller, C.; Gidt, W.; Sun, Y.; Demeshko, S.; Meyer, F.; Sitzmann, H. Iron(III) High-Spin and Low-Spin Complexes from Pentaisopropylcyclopentadienyliron(II) Bis(rimethylsilyl)amide. *Eur. J. Inorg. Chem.* **2017**, *2017*, 3635−3643. (c) Walter, M. D.; White, P. S. $[\{Cp'Fe(\mu\text{-}OH)\}_3]$: the Synthesis of a Unique Organometallic Iron Hydroxide. *Dalton Trans.* **2012**, *41*, 8506−8508. (d) Reiners, M.; Maekawa, M.; Daniliuc, C. G.; Freytag, M.; Jones, P. G.; White, P. S.; Hohenberger, J.; Sutter, J.; Meyer, K.; Maron, L.; Walter, M. D. Reactivity Studies on $[Cp'Fe(\mu\text{-}I)]_2$: nitrido-, sulfido-, and diselenide iron complexes derived from pseudohalide activation. *Chem. Sci.* **2017**, *8*, 4108−4122.
(36) Shafi, K. V. P. M.; Ulman, A.; Yan, X.; Yang, N.-L.; Estournès, C.; White, H.; Rafailovich, M. Sonochemical Synthesis of Functionalized Amorphous Iron Oxide Nanoparticles. *Langmuir* **2001**, *17*, 5093.
(37) (a) Bouwman, E.; van Gorkum, R. A Study of New Manganese Complexes as Potential Driers for Alkyd Paints. *J. Coat. Technol. Res.* **2007**, *4*, 491−503. (b) Preininger, O.; Honziček, J.; Kalenda, O.; Vinklárek, J. Drying Activity of Oxovanadium(IV) 2-Ethylhexanoate in Solvent-borne Alkyd Paints. *J. Coat. Technol. Res.* **2016**, *13*, 479−487.
(38) Pryor, W. A.; Prier, D. G.; Church, D. F. Radical Production from the Interaction of Ozone and PUFA as Demonstrated by Electron Spin Resonance Spin-Trapping Techniques. *Environmental Research* **1981**, *24*, 42−52.
(39) Dikalov, S. I.; Mason, R. P. Spin Trapping of Polyunsaturated Fatty Acid-Derivatived Peroxyl Radicals: Reassignment to Alkoxyl Radical Adducts. *Free Radical Biol. Med.* **2001**, *30*, 187−197.
(40) Gezici-Koç, Ö.; Thomas, C. A. A. M.; Michel, M.-E. B.; Erich, S. J. F.; Huinink, H. P.; Flapper, J.; Duivenvoorde, F. L.; van der Ven, L. G. J.; Adan, O. C. G. In-depth Study of Drying Solvent-Borne Alkyd Coatings in Presence of Mn- and Fe- based Catalysts as Cobalt Alternatives. *Materials Today Communications* **2016**, *7*, 22−31.
(41) Oyman, Z. O.; Ming, W.; van der Linde, R.; ter Borg, J.; Schut, A.; Bieleman, J. H. Oxidative Drying of Alkyd Paints Catalysed by a Dinuclear Manganese Complex (MnMeTACN). *Surface Coatings International Part B: Coatings Transactions* **2005**, *88*, 269−275.
(42) Erich, S. J. F.; Laven, J.; Pel, L.; Huinink, H. P.; Kopinga, K. Comparison of NMR and Confocal Raman Microscopy as Coatings Research Tools. *Prog. Org. Coat.* **2005**, *52*, 210−216.
(43) Muik, B.; Lendl, B.; Molina-Díaz, A.; Ayora-Cañada, M. J. Direct Monitoring of Lipid Oxidation in Edible Oils by Fourier Transform Raman Spectroscopy. *Chem. Phys. Lipids* **2005**, *134*, 173−182.
(44) Ellis, G.; Claybourn, M.; Richards, S. E. The Application of Fourier Transform Raman Spectroscopy to the Study of Paint Systems. *Spectrochimica Acta Part A: Molecular Spectroscopy* **1990**, *46*, 227−241.
(45) (a) Nardelli, F.; Martini, F.; Lee, J.; Lluvears-Tenorio, A.; La Nasa, J.; Duce, C.; Ormsby, B.; Geppi, M.; Bonaduce, I. The Stability of Paintings and the Molecular Structure of the Oil Paint Polymeric Network. *Sci. Rep.* **2021**, *11*, 14202. (b) Pizzimenti, S.; Bernazzani, L.; Tinè, M. R.; Treil, V.; Duce, C.; Bonaduce, I. Oxidation and Cross-Linking in the Curing of Air-Drying Artists' Oil Paint. *ACS Appl. Polym. Mater.* **2021**, *3*, 1912−1922. (c) Bonaduce, I.; Duce, C.; Lluveras-Tenorio, A.; Lee, J.; Ormsby, B.; Burnstock, A.; van den Berg, K. J. Conservation Issues of Modern Oil Paintings: A Molecular Model on Paint Curing. *Acc. Chem. Res.* **2019**, *52*, 3397−3406.

https://doi.org/10.1021/jacsau.1c00579
JACS Au 2022, 2, 531−540